RSC Advances

PAPER

View Article Online
View Journal | View Issue

Cite this: *RSC Adv.*, 2015, **5**, 72051

Laser desorption ionization (LDI) silicon nanopost array chips fabricated using deep UV projection lithography and deep reactive ion etching

Nicholas J. Morris,[a] Heather Anderson,[a] Brian Thibeault,[b] Akos Vertes,[c] Matthew J. Powell[a] and Trust T. Razunguzwa[a]

Received 22nd June 2015
Accepted 20th August 2015

DOI: 10.1039/c5ra11875a

www.rsc.org/advances

Deep UV projection lithography (DUV-PL) and deep reactive ion etching (DRIE) processes are used to fabricate silicon nanopost surfaces for laser desorption ionization mass spectrometry (LDI-MS). Described here is a fabrication process that is amenable to mass production of silicon nanopost array (NAPA) devices optimized for laser desorption ionization mass spectrometry of small molecules less than 2 kDa, suitable for pharmaceutical and metabolomics applications. The resulting devices exhibit excellent performance for analysis and quantitation of pharmaceutical drugs over at least four orders of magnitude dynamic range, with very good limits of detection and lower limits of quantitation. For metabolite analysis, these devices also exhibit improved spectral quality over MALDI-MS which suffers from noise from the chemical matrix. With the ability to perform a one-step sample spotting, these devices become extremely useful for high throughput workflows afforded by MALDI mass spectrometry platforms.

Introduction

Laser desorption ionization mass spectrometry (LDI-MS) has significantly transformed the analysis of biomolecules over the last 3 decades. The most common of the LDI-MS methods first reported in 1985 is matrix assisted laser desorption ionization mass spectrometry (MALDI),[1] which makes use of an organic matrix to promote soft ionization of molecules. MALDI is a well-established, sensitive and high throughput technique, that is effective in the analysis of large molecules, especially molecular profiling of proteins, peptides, oligosaccharides and oligonucleotides. MALDI-MS has been a very effective tool in genomic, proteomic, metabolomic and clinical research.[2] In recent times, MALDI has been effectively used for mass spectrometry imaging of macromolecules from a variety of sample sources including animal tissues. However, MALDI has not been extensively used for analysis of small molecules such as pharmaceutical drugs, small peptides, or small molecule natural products, due to the interference of the chemical noise from the matrix in the low mass region <700 Da. More-so, the co-crystallization of sample and chemical matrix can result in non-homogenous spots, giving rise to poor spot to spot reproducibility. These limitations have led to the development of many surface-enhanced ionization techniques, which allow for desorption and ionization of small molecules without the chemical matrix.[3] Other researchers have developed methods such as label-assisted LDI-MS where analytes are labeled with a UV-absorbing polyaromatic chemical tag, reacted and reaction products containing the tag detected by LDI-MS.[4–6]

Surface Assisted Laser Desorption Ionization (SALDI) techniques make use of either inorganic nanoparticles[7] or structured surfaces to provide a means of desorption and ionization of molecules. Inorganic nanoparticles for LDI are mainly based on metals such as gold,[8,9] silver, or platinum.[10–13] Also used are semiconductor materials such as germanium, zinc oxide,[14] tungsten oxide[15] or silicon particles. On the other hand, structured surfaces involve fabricating features such as nanowires,[16,17] nanoposts,[18] nanocones,[19] nanowells[20] and nanotubes on inorganic materials such as silicon or germanium. The most common commercial products previously on the market for matrix-free LDI-MS are nano-assisted laser desorption ionization (NALDI),[21–23] direct ionization on silicon (DIOS)[24,25] and nanoparticle initiated mass spectrometry (NIMS)[26] devices. The desorption and ionization on SALDI materials heavily relies on the interaction of the laser radiation with these surfaces or materials, resulting in the absorption of energy that is transferred to molecules deposited on the surface. Although the actual mechanism of desorption/ionization is not yet well-understood, this photo-absorption process is thought to be very important for the desorption/ionization of the analyte, controlled by electronic, thermal and field effects, emanating from interaction of the laser radiation with electrons of surface material.[18]

[a]*Protea Biosciences Inc., 1311 Pineview Drive, Suite 501, Morgantown, WV, 26505, USA. E-mail: trust.razunguzwa@proteabio.com*

[b]*University of California Santa Barbara (UCSB), ESB Room 1109, Santa Barbara, CA, 93106, USA*

[c]*George Washington University, Dept of Chemistry, 800 22nd St N. W. Washington, DC, 20052, USA*

A significant amount of work has been reported for NIMS and DIOS substrates.[27–31] Both NIMS and DIOS substrates are based on porous silicon, but differ in wafer dopant, pore size, depth, and surface chemistry.[32] NIMS and DIOS substrates are mesoporous (>10 μm pore depth) and macroporous (50–100 nm pore depth) p-type silicon respectively. DIOS substrates are modified with perfluorinated silane, whereas NIMS substrates are functionalized with highly fluorinated siloxane. Fluorination of DIOS substrate stabilizes the Si–H surface resulting from the etching process, which can be oxidized over time. Because of the electrochemical etching process used to produce both the DIOS and NIMS substrates, the batch to batch reproducibility of the substrate is difficult to control.[27,32,33] Variations in fabrication yield changes in structure dimensions, thus producing varying results in analyte detection. In addition, DIOS has been shown to have a limited shelf-life before oxidation of the device has a negative effect. In the same manner, NALDI nanowires are functionalized with 3-(pentafluorophenyl)propyl dimethylchlorosilane ($C_{11}H_{12}ClF_5Si$), and introduced on stainless steel substrate *via* liquid solid vapor deposition. NALDI devices have very low laser fluence threshold compared to DIOS or MALDI matrices. As the laser fluence is increased, NALDI spectra become more and more complex due to cluster ion formation and melting of the nanowires.[32] This makes NALDI spectra not very useful at high laser energy.

Development of NAPA technology was designed to improve upon these limitations demonstrated by DIOS, NIMS, and NALDI for small molecule analysis by LDI-MS. NAPA devices utilize highly-ordered silicon nanoposts. The production process allows for generation of consistent structure dimensions and periodicity that yield reproducible response of analytes spotted on the posts. The structure dimensions and periodicity have been optimized for maximum sensitivity of small molecules. NAPA has demonstrated phenomenal detection limits with zeptomole quantities spotted on the target detected on these devices, and have since been applied to analysis a small cell populations.[34–36] In addition, unlike NALDI, NAPA substrates offer very little analyte fragmentation at low fluence, and as laser fluence increases, there is greater fragmentation of the analyte against clean spectral background, resulting in usable spectra for structural elucidation.

Although NAPA devices clearly show benefits for small molecule analysis by LDI-MS, large scale production of the devices has been limited. NAPA devices developed in previous work have been fabricated using e-beam lithography (EBL) for pattern transfer, followed by reactive ion etching. The EBL process is very slow and expensive. Only small arrays can be fabricated at time, and the process is not easily scalable. The motivation for this work was therefore the need for a fabrication process that can be used to mass produce NAPA devices, but maintain the performance characteristics and reproducibility that have been reported for EBL NAPA chips. Other research groups have attempted several processes which have included sample patterning using colloidal lithography with polystyrene nanospheres,[19] metal evaporation, superionic solid state stamping (S4),[37] followed by metal assisted chemical etching (MacEtch)[38,39] or reactive ion etching. Although the sample patterning methods are low cost, they also cannot be easily scaled-up for mass production. In addition, there is significant variation in structure dimensions and periodicity.

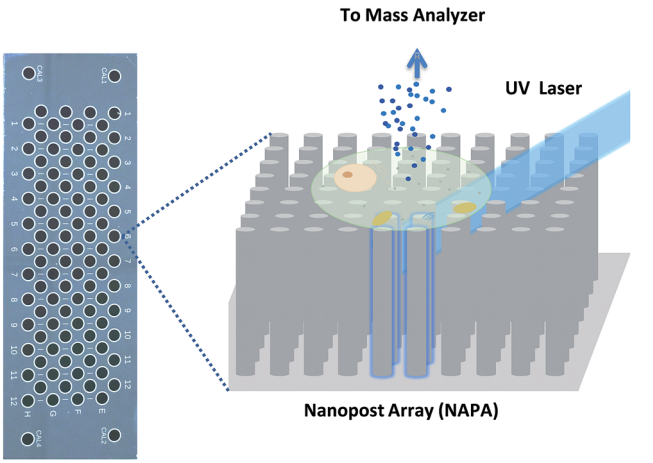

Fig. 1 On the left is an optical image of a NAPA-LDI-MS chip showing nanopost array target spots. Shown on the right is a schematic diagram of the nanopost array laser desorption ionization process where a UV laser beam from a MALDI mass spectrometer is absorbed by the nanoposts, allowing ionization of the sample.

Patterning using DUV-PL offers a fast, high resolution fabrication technique that forms very uniform structures on the surface (Fig. 1). NAPA devices which have a post diameter of 100–150 nm, a periodicity of 337 nm and aspect ratios ≥10 have been shown to give optimum ion yield for laser desorption ionization experiments.[34] Using DUV-PL, nanopost arrays of these dimensions are rapidly and reproducibly patterned on silicon, and the nanoposts are formed using reactive ion etching. Thus, this technique will allow for a cost effective production method of the NAPA device that can easily be scaled-up for mass production without sacrificing the reproducibility of the structure dimensions or periodicity.

Experimental

Materials and methods

Analytical reference small molecule standards and isotopes, metoprolol (d7), ropivacaine (d7), and clonidine (d4) were purchased from CDN Isotopes (Canada). Metoprolol, nordiazepam (d5), chlorpheniramine (d6), fentanyl (d5), buprenorphine (d4), norbuprenorphine (d3), and amiodarone (d4) were purchased from Cerilliant (Round Rock, TX). Verapamil was purchased from Sigma Aldrich (St Louis, MO). Chlorpheniramine maleate, clonidine, and ropivacaine were purchased from USP Reference Standards (Rockville, MD). Two small molecule mixtures (amiodarone, buprenorphine, clonidine, ropivacaine, and verapamil) were generated in 10% acetonitrile at 1 ng and 31 pg for each small molecule per microliter. A volume of 1 μL was directly spotted onto both NAPA and MALDI targets. Calibration solutions were created for each small molecule with a dynamic range more than 4 orders of magnitude (1 pg to 10 ng). Calibration standards were produced in

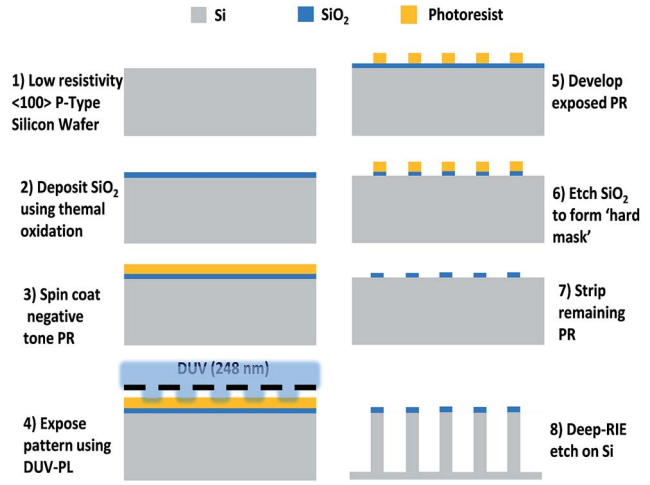

Fig. 2 Schematic diagram of the fabrication process of a NAPA-LDI-MS chip.

10% acetonitrile solution and 1 μL was directly spotted onto a NAPA target for analysis. A selection of the buprenorphine standards were also spotted for both NAPA and MALDI for spot imaging. Spot deposit size for imaging was 0.5 μL. All MALDI spots were also spotted with 1 μL of 10 mg mL^{-1} CHCA MALDI matrix from Protea Biosciences (Morgantown, WV).

Low resistivity (0.005–0.1 Ω cm)[40] p-type silicon wafers were purchased from Silicon Valley Microelectronics, Inc. (Santa Clara, CA). Shipley AR2-600 anti-reflective coating and UVN-2300-0.5 negative tone photoresist were purchased from DOW (Newark, DE). Post-exposure development of photoresists was performed using AZ300MIF (0.26 TMAH-based developer, no surfactant), from AZ Electronic Materials (Somerville, NJ).

NAPA fabrication

Fabrication on silicon wafers was performed using DUV-PL and followed by DRIE as shown in Fig. 2. Fabrication was performed at the University of California Santa Barbara (UCSB) Nanotechnology Facility. A silicon dioxide layer was initially deposited on batches of virgin Si wafers using dry oxidation in a tube furnace at 1050 °C for 90 minutes. This oxide layer (~115 nm) acts as a "hard mask" to protect the Si underneath during etching. After the SiO_2 layer was grown, wafers were spin-coated with an anti-reflective coating at 3500 rpm for 30 seconds, followed by a hot plate bake at 220 °C for 60 seconds. Next, UVN-2300-0.5 DUV photoresist was deposited using spin coating at 3500 rpm for 30 seconds. A soft bake was performed on a hot plate at 110 °C for 90 seconds.

Projection exposure of the nanopost pattern was achieved using an ASML 5500/300 248 nm DUV stepper (Veldhoven, AN) with 4× reduction optics. A post exposure bake was performed at 105 °C for 60 seconds. The nanopost array pattern was developed using AZ300MIF developer for 22 seconds. Post-development, wafers were rinsed in deionized water for 60 seconds and dried using N_2 gas.

The etching protocol was carried out in four steps. Initial etching steps were performed in a Panasonic E640 ICP-RIE instrument (Rolling Meadows, IL) to form the SiO_2 hard mask. A summary of the etching parameters can be found in Table 1. The final etch was achieved using a deep Si RIE chamber manufactured by PlasmaTherm (Saint Petersburg, FL). A single-step vertical Si etch was performed with a chamber pressure of 19 mT, a ICP power of 825 W and an RIE power of 15 W for 9 minutes. The mixture of etchant gases used was as follows: C_4F_8, SF_6, and Ar at 52 sccm, 28 sccm, and 20 sccm, respectively.

Static contact angle measurements were performed to characterize the wetting properties NAPA surfaces. Drops (~2 μL) of deionized water were placed on the sample's surface. Images of the droplets were taken using a fixed microscope. The image was digitally analyzed using the Image J "drop analysis" plugin method LB-ADSA (National Institutes of Health). X-ray photoelectron spectroscopy (XPS) was used to analyze chemical composition. XPS was conducted on a Physical Electronics PHI 5000 VersaProbe system (Chanhassen, MN). The X-ray beam was 100 μm, 25 W, and 15 kV, from an A1 Kα source with a photon energy of 1486.6 eV. Spectra were collected from F 1s, C 1s, O 1s, Si 2p, and Cr 1s levels, with pass energy of 93 eV, energy step of 0.2 eV, and time/step of 50 ms. Spectra were collected with multiple repeats and the data averaged.

MALDI-TOF analysis

Mass spectrometry analysis was performed using the AB Sciex 4800 MALDI TOF/TOF instrument (Framingham, MA) in positive ion reflector mode using laser energy between 1800–2500. All quantitation data was collected in batch mode with center bias selected. Delay times were set between 200–600 optimizing detection for each analyte. MS imaging data was collected at 250 μm pitch.

Results and discussion

Characterization of nanopost arrays

Past research on nanopost array devices for laser desorption ionization used electron beam lithography (EBL) followed by DRIE for fabrication of nanoposts on silicon.[34] These devices

Table 1 Etching parameters for SiO_2 hard mask

Step	O_2 (sccm)	CHF_3 (sccm)	Press (Pa)	ICP P (W)	RIE P (W)	Time (s)
ARC	40	0	0.5	75	75	40
SiO_2	5	45	0.5	500	100	80
PR/ARC strip	40	0	0.5	200	100	200

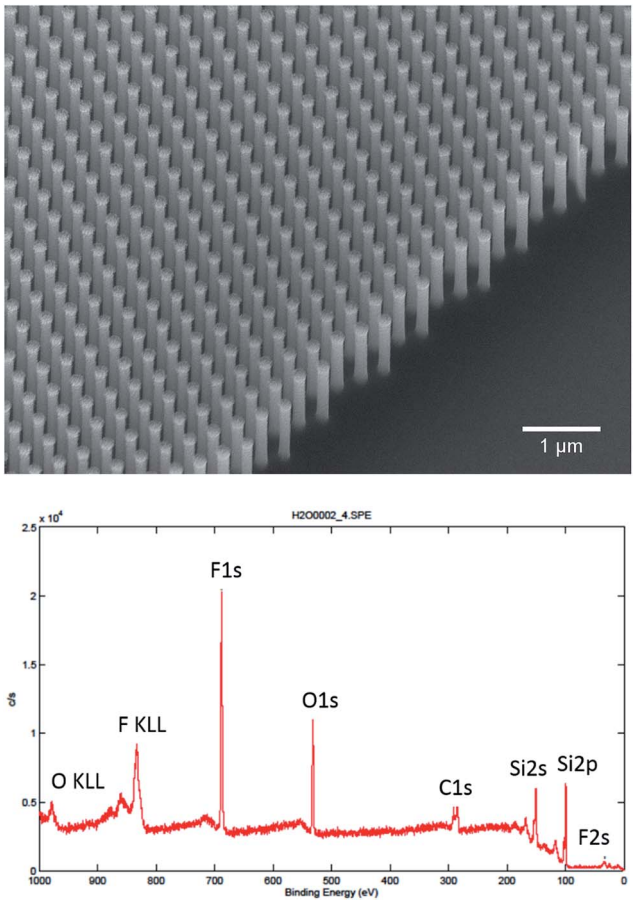

Fig. 3 The top panel is an SEM image of nanopost arrays fabricated using DUV-PL and DRIE. The nanoposts are ~1 μm high, 150 nm in diameter, and have a periodicity of 337 nm. The bottom image is an X-ray photoelectron spectroscopy (XPS) spectrum of the nanopost array surface, showing significant degree of surface fluorination.

have been carefully characterized to optimize the factors that maximize ion yield for LDI-MS. It was shown that there are three main features of the nanopost arrays that have been determined as important for an optimum NAPA LDI-MS surface, namely: (1) well-ordered nanopost arrays, (2) dimensions that maximize laser light absorption and subsequent resonance effects that promote analyte desorption and ionization (3) a highly fluorous surface to maximize analytical sensitivity.[41] In this work, nanoposts with these characteristic features have been fabricated using DUV-PL and DRIE processes as shown in the SEM and XPS images in Fig. 3. The surface structure of NAPA was characterized using SEM which revealed well-ordered nanoposts with a periodicity of ~337 nm, diameter of ~150 nm and ~1.2 μm in depth (aspect ratio of 8), consistent with the optimized, previously fabricated EBL NAPA devices. These dimensions are consistent with the EBL-NAPA optimized nanopost dimensions for enhanced ion production *via* resonance-like behavior upon interaction of laser light with the nanostructures. It was also determined for the EBL NAPA that ion yield increases with aspect ratio. A depth of 1.2 μm fabricated here, represents the upper end of the depth that currently can be etched on silicon using DRIE, while maintaining good side wall definition. In addition, laser light confinement effects (field enhancements, high heating rates, prolonged interaction times) promote sample ionization in the nanostructures, and a periodicity of 337 nm was determined to be optimum for coupling the laser light of a similar wavelength.[34]

The surface chemistry of the nanoposts was characterized by XPS. The XPS image in Fig. 3 shows a significant degree of fluorination from the DRIE process which uses C_4F_8/SF_6 gas as the reactive ion etching mixture. DRIE is an anisotropic etching process which allows deep penetration into the surface creating steep, vertical side-walls shown in the SEM image in Fig. 3. DRIE allows for high aspect ratio structures necessary to achieve high ion yield during mass spectrometry analysis. With the gases used for etching, a 1–5 atom fluorous layer develops on the side-walls during etching which protects the side-walls from lateral etching. When compared to nanoposts fabricated by e-beam lithography and DRIE, the DUV-PL nanoposts showed very similar elemental composition as EBL NAPA chips. As shown in Table 2, both chips have considerable level of fluorination (~30%), a characteristic that make them super-hydrophobic (contact angles between 140 and 150), and helps concentrate the sample spotted on the targets to a very small area on the chip, thereby enhancing analytical sensitivity. Silanol groups still remain on both EBL and DUV-PL surfaces as the evidenced by the oxygen level at 17.2 and 22.7% for EBL and DUV-PL chips, respectively.

It has been reported that silanol groups are an important proton source for ionization, with the presence and electronegativity of fluorine increasing the acidity of the silanol group for increased analyte sensitivity. This observation has also been made for DIOS and NALDI surfaces.[27]

Spectral quality

One of the major advantages of NAPA surfaces is the ability to acquire mass spectra in the low mass regions without the addition of external chemical matrix. Traditional MALDI analysis utilizes a chemical matrix which enhances the ability to ionize a sample. This method is extremely useful when analyzing molecules over 1000 Da. However, the chemical matrix generates a large amount of interfering peaks between the mass range of 100 to 1000 *m*/*z*. Clean mass spectra of small molecules can be acquired by NAPA for single component or small molecule mixtures in the low mass range were chemical matrix is generally interfering with MALDI analysis. Fig. 4A demonstrates the difference between mass spectra for MALDI-MS and NAPA-LDI-MS for select small molecule compounds at

Table 2 XPS measurement for EBL and DUV-PL chips

XPS-measured atomic concentrations (%)					
	C	O	F	Si	Cr
EBL NAPA surface	39.1	17.2	30.6	11	2.1
DUV-HM NAPA surface	37.1	22.7	30.9	9.3	0

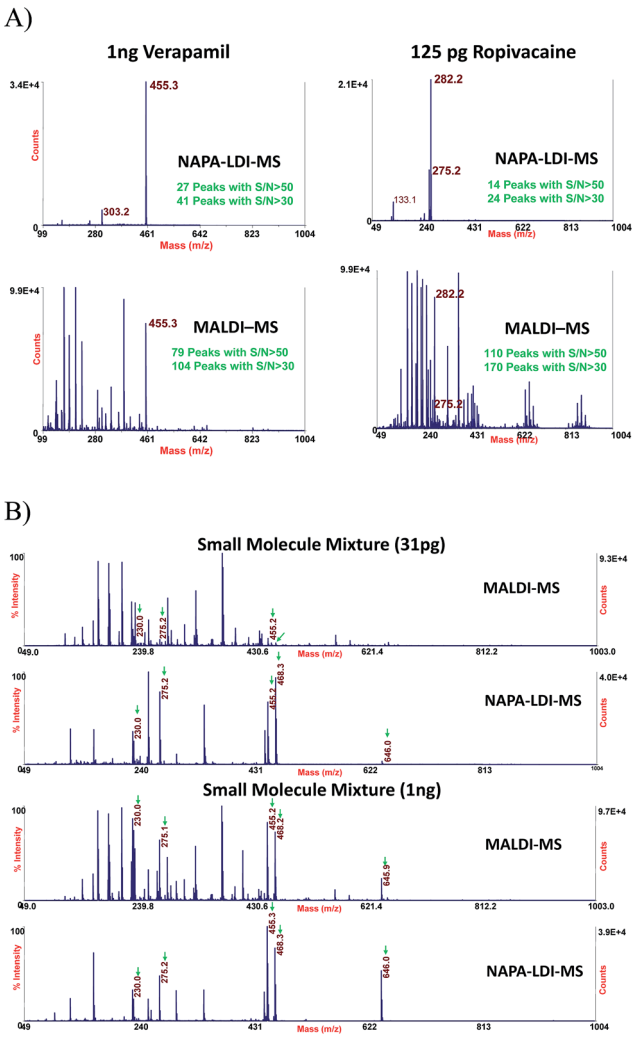

Fig. 4 (A) Nanopost array LDI-MS spectra compared to MALDI-MS spectra of small molecule drugs verapamil and ropivacaine, showing a significant reduction in background signal for nanopost array case. The background peaks for MALDI-MS dominate the spectrum, whereas for the nanopost array spectrum, the analyte peak is the most dominant with low signal/noise values for the background peaks. (B) Shows MALDI mass spectra compared to NAPA-LDI mass spectra for a mixture of small molecules comprising of verapamil (455), amiodarone (646), buprenorphine (468), ropivacaine (275), clonidine (230). There are significantly lower background peaks for the NAPA spectra, and the major peaks are either the small molecule, or a fragment of the molecule.

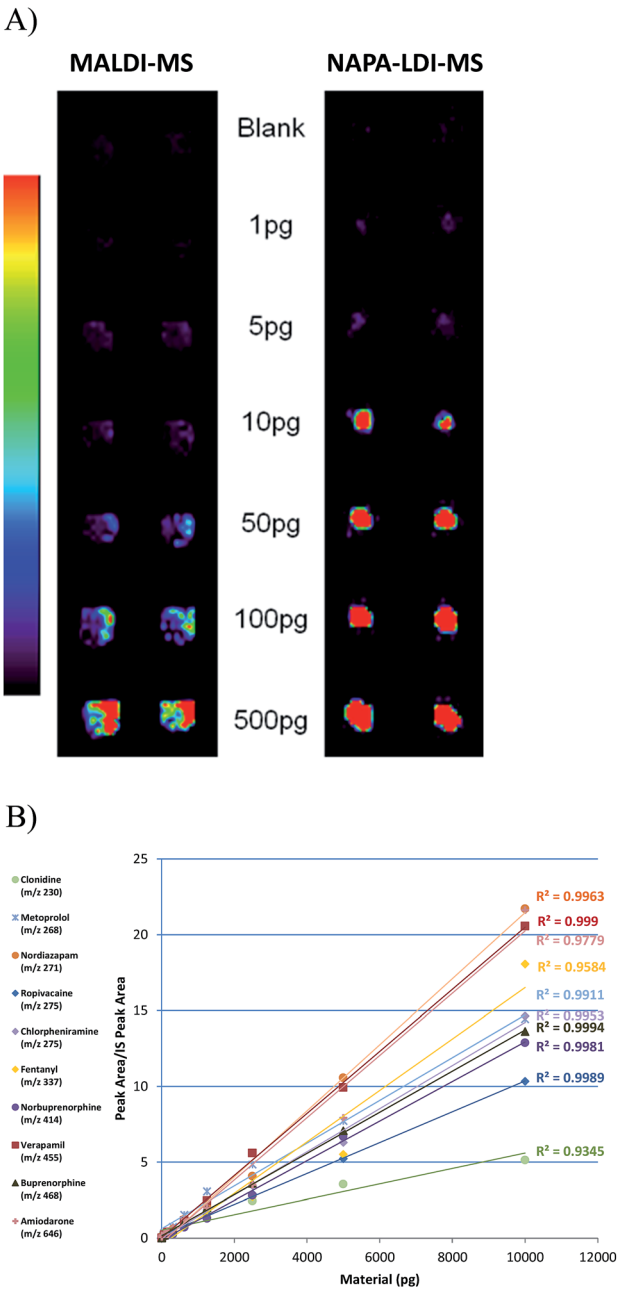

Fig. 5 (A) Buprenorphine ion maps (*m*/*z* 468.2) showing distribution on NAPA and MALDI targets. (B) Calibration curves for 10 different small molecules showing excellent linearity over 4 orders of magnitude dynamic range from 1 pg to 10 ng, (~2 fmol to 20 pmol for buprenorphine). These results are for samples spotted in 1 μL volume.

different concentrations. The two mass spectra on the left were acquired from 1 ng of the drug verapamil (*m*/*z* 455) spotted on NAPA, and on stainless steel MALDI targets, spotted with CHCA matrix. The NAPA spectrum has one high intensity verapamil molecular ion peak, and smaller peaks at *m*/*z* 303, 260, 165, 150 which are fragments of verapamil. Higher intensities from these fragments can be achieved by using higher laser energy. Verapamil is detected in the MALDI-MS case, but along with numerous matrix cluster peaks. At S/N threshold of 50, 27 peaks were detected for NAPA-LDI-MS compared to 79 for MALDI-MS. In the same manner, the two spectra on the right hand side is a comparison of a different drug, ropivacaine (*m*/*z* 275) spotted at a lower amount of 125 pg. This drug was spotted together with its d7 version (*m*/*z* 282) used as internal at 500 pg level. In this case, there were only 14 peaks in NAPA-LDI-MS spectrum compared to 110 peaks in the MALDI mass spectrum, also due to the presence of matrix clusters. When a mixture of drugs (clonidine, ropivacaine, buprenorphine, verapamil and amiodarone) were used for a similar experiment (Fig. 4B), consistent results were achieved, where the MALDI spectra were much

Table 3 RSD and % accuracy values for quantitation of 10 small molecules between 200 and 700 Da mass range

	$N =$	Average RSD	% accuracy LQC	% accuracy MQC	% accuracy HQC
Buprenorphine	3	7.2	126.6	102.3	98.6
Norbuprenorphine	3	9.5	120.1	102.3	101.9
Ropivacaine	5	8.6	128.0	122.6	112.2
Amiodarone	3	9.3	103.8	109.3	112.3
Chlorpheniramine	4	10.6	136.8	94.8	99.9
Fentanyl	4	10.1	114.6	145.3	109.4
Clonidine	4	11.1	96.0	99.7	105.5
Nordiazepam	4	12.3	98.5	107.7	102.5
Metoprolol	4	18.2	NA	100.8	101.0
Verapamil	3	24.0	92.2	103.3	101.2

more complex than the NAPA-LDI-MS spectra. In the NAPA spectra, the molecular ion peaks for the drugs dominated the spectra where as for MALDI-MS the spectra were dominated by matrix clusters at both amount of 31 pg and 1 ng spotted.

Quantitation of small molecules

To determine the distribution of analyte for samples spotted on NAPA targets, buprenorphine varying from 1–500 pg were spotted on NAPA and MALDI targets, MALDI-MS and NAPA-LDI-MS ion maps representing distribution of buprenorphine (468.2 m/z) on the spot were generated in Tissueview imaging software (Fig. 5A). The images clearly show a smaller well distributed spot for the NAPA image, whereas the MALDI spots spread further outside of the target area. The sample droplet for the NAPA-LDI-MS case is confined to a small footprint on the NAPA spot resulting in concentration of analyte in a smaller area, translating into higher sensitivity. In addition, it is apparent that MALDI spots have a tendency to exhibit variable signal within a single spot depending on how well and homogenous the matrix crystallizes. NAPA spots in contrast when spotted out of aqueous or low organic solution tend to dry toward the center (due to the highly hydrophobic surface) into a concentrated spot which gives homogenous signal across the spot.

The fabricated NAPA-LDI-MS chips were used to quantitate small pharmaceutical drug molecules. Each chip is comprised of 96 NAPA spots, 2 mm in diameter. A single chip was used to spot calibrants and samples used to determine accuracy, reproducibility, linearity of the dynamic range, and detection limit for these small molecules. In every case of the 10 molecules shown in Fig. 5B, 4 orders of magnitude for quantitation were achieved, with detection limits close to 1 pg, delivered in 1 μL of solution. Each amount plotted in the figure was spotted in replicates, on three or more different NAPA spots. An average ratio of the sample to internal standard (isotope of sample) peak areas was plotted against the amount spotted. In most cases, the % RSDs from spot to spot was less than 15%, except verapamil where isotopic internal standard was not used. For the most part, % accuracies were within ±15% for the low, medium and high amount QC samples, see Table 3.

Conclusions

A new process utilizing deep UV projection lithography and reactive ion etching for fabricating LDI-MS silicon nanoposts is presented. This process makes NAPA devices amenable to mass production, facilitated by rapid transfer of nanopost patterns *via* DUV-PL. The fabricated features were characterized by SEM, XPS, and contact angle measurements all of which show great similarity with NAPA devices previously fabricated using e-beam lithography, and successfully used for metabolomics studies. For mass spectrometry analysis, the NAPA devices fabricated here do not require a chemical matrix for analysis of small molecules, producing high quality mass spectra, with minimum fragmentation useful for small molecule quantitation.

Acknowledgements

We thank the Vertes group at George Washington University for providing EBL NAPA chips. We also acknowledge West Virginia University Research Corporation for access to the research shared facilities that allowed us to dice silicon wafers, as well as perform XPS and SEM measurements. This Research was sponsored by the U.S. Army Research Office and the Defense Advanced Research Projects Agency and was accomplished under Cooperative Agreement Number W911NF-14-2-0020. The views and conclusions contained in this document are those of the authors and should not be interpreted as representing the official policies, either expressed or implied, of the Army Research Office, DARPA, or the U.S. Government.

References

1 M. Karas, D. Bachmann and F. Hillenkamp, *Anal. Chem.*, 1985, 2935.
2 W. Y. Ng Eddy, Y. M. Wong Melody and C. W. Poon Terence, *Top. Curr. Chem.*, 2014, **336**, 139.
3 Arakawa R., Kinzoku Nano/Maikuro Ryushi no Keijo/Kozo Geigyo Gijutsu, 2009, 249.
4 J. R. Cabrera-Pardo, D. I. Chai, S. Liu, M. Mrksich and S. A. Kozmin, *Nat. Chem.*, 2013, **5**, 423.

5 A. B. Partha Sarathi Addy, S. M. Mandala and A. Basak, *RSC Adv.*, 2014, **4**, 46555.
6 S. B. R. Partha Sarathi Addy, S. M. Mandal and A. Basak, *RSC Adv.*, 2014, **4**, 23314.
7 W.-T. Chen, I. Tomalova, J. Preisler and H.-T. Chang, *J. Chin. Chem. Soc. (Taipei, Taiwan)*, 2011, **58**, 769.
8 I. Tomalova, C.-H. Lee, W.-T. Chen, C.-K. Chiang, H.-T. Chang and J. Preisler, *J. Am. Soc. Mass Spectrom.*, 2013, **24**, n305.
9 T. Yonezawa, H. Kawasaki, A. Tarui, T. Watanabe, R. Arakawa, T. Shimada and F. Mafune, *Anal. Sci.*, 2009, **25**, 339.
10 M. Cueto, M. Piedrahita, C. Caro, B. Martinez-Haya, M. Sanz, M. Oujja and M. Castillejo, *J. Phys. Chem. C*, 2014, **118**, 11432.
11 H. Kawasaki, T. Yao, T. Suganuma, K. Okumura, Y. Iwaki, T. Yonezawa, T. Kikuchi and R. Arakawa, *Chem.–Eur. J.*, 2010, **16**, 10832.
12 H. Kawasaki, T. Ozawa, H. Hisatomi and R. Arakawa, *Rapid Commun. Mass Spectrom.*, 2012, **26**, 1849.
13 S. Nitta, H. Kawasaki, T. Suganuma, Y. Shigeri and R. Arakawa, *J. Phys. Chem. C*, 2013, **117**, 238.
14 A. A. Grechnikov, V. B. Georgieva, S. S. Alimpiev, A. S. Borodkov, S. M. Nikiforov, Y. O. Simanovsky, D. Dimova-Malinovska and O. I. Angelov, *J. Phys.: Conf. Ser.*, 2010, **223**, 012038.
15 X. Yang, X. K. Hu, A. V. Loboda and R. H. Lipson, *Adv. Mater. (Weinheim, Ger.)*, 2010, **22**, 4520.
16 E. P. Go, J. V. Apon, G. Luo, A. Saghatelian, R. H. Daniels, V. Sahi, R. Dubrow, B. F. Cravatt, A. Vertes and G. Siuzdak, *Anal. Chem.*, 2005, **77**, 1641.
17 W.-J. Shin, J.-H. Shin, J.-Y. Song and S.-Y. Han, *J. Am. Soc. Mass Spectrom.*, 2010, **21**, 989.
18 B. N. Walker, T. Razunguzwa, M. Powell, R. Knochenmuss and A. Vertes, *Angew. Chem., Int. Ed.*, 2009, **48**, 1669.
19 Y. Wang, Z. Zeng, J. Li, L. Chi, X. Guo and N. Lu, *J. Am. Soc. Mass Spectrom.*, 2013, **24**, 66.
20 B. Gulbakan, D. Park, M. Kang, K. Kececi, C. R. Martin, D. H. Powell and W. Tan, *Anal. Chem. (Washington, DC, U. S.)*, 2010, **82**, 7566.
21 A. Tata, A. M. A. P. Fernandes, V. G. Santos, R. M. Alberici, D. Araldi, C. A. Parada, W. Braguini, L. Veronez, G. Silva Bisson, F. H. Z. Reis, L. C. Alberici and M. N. Eberlin, *Anal. Chem. (Washington, DC, U. S.)*, 2012, **84**, 6341.
22 R. H. Daniels, S. Dikler, E. Li and C. Stacey, *JALA*, 2008, **13**, 314.
23 M. F. Wyatt, S. Ding, B. K. Stein, A. G. Brenton and R. H. Daniels, *J. Am. Soc. Mass Spectrom.*, 2010, **21**, 1256.
24 Z. Shen, J. J. Thomas, C. Averbuj, K. M. Broo, M. Engelhard, J. E. Crowell, M. G. Finn and G. Siuzdak, *Anal. Chem.*, 2001, **73**, 612.
25 J. Wei, J. M. Buriak and G. Siuzdak, *Nature (London)*, 1999, **399**, 243.
26 T. R. Northen, O. Yanes, M. T. Northen, D. Marrinucci, W. Uritboonthai, J. Apon, S. L. Golledge, A. Nordstroem and G. Siuzdak, *Nature (London, U. K.)*, 2007, **449**, 1033.
27 K. P. Law and J. R. Larkin, *Anal. Bioanal. Chem.*, 2011, **399**, 2597.
28 D. Y. Lee, V. Platt, B. Bowen, K. Louie, C. A. Canaria, C. T. McMurray and T. Northen, *Integr. Biol.*, 2012, **4**, 693.
29 W. Reindl and T. R. Northen, *Anal. Chem. (Washington, DC, U. S.)*, 2010, **82**, 3751.
30 G. J. Patti, L. P. Shriver, C. A. Wassif, H. K. Woo, W. Uritboonthai, J. Apon, M. Manchester, F. D. Porter and G. Siuzdak, *Neuroscience (Amsterdam, Neth.)*, 2010, **170**, 858.
31 K. P. Law, *Int. J. Mass Spectrom.*, 2010, **290**, 47.
32 T. Guinan, M. Ronci, R. Vasani, H. Kobus and N. H. Voelcker, *Talanta*, 2015, **132**, 494.
33 K. P. Law, *Int. J. Mass Spectrom.*, 2010, **290**, 72.
34 B. N. Walker, J. A. Stolee, D. L. Pickel, S. T. Retterer and A. Vertes, *J. Phys. Chem. C*, 2010, **114**, 4835.
35 B. N. Walker, J. A. Stolee and A. Vertes, *Anal. Chem.*, 2012, **84**, 7756.
36 B. N. Walker, C. Antonakos, S. T. Retterer and A. Vertes, *Angew. Chem.*, 2013, **52**, 3650.
37 K. H. Hsu, P. L. Schultz, P. M. Ferreira and N. X. Fang, *Nano Lett.*, 2007, **7**, 446.
38 W. Zhang, X. Fan, S. Sang, P. Li, G. Li, Y. Sun and J. Hu, *Korean J. Chem. Eng.*, 2013, **31**, 62.
39 Z. Huang, N. Geyer, P. Werner, J. de Boor and U. Gosele, *Adv. Mater. (Deerfield Beach, Fla.)*, 2011, **23**, 285.
40 S. Alimpiev, A. Grechnikov, J. Sunner, V. Karavanskii, Y. Simanovsky and S. Nikiforov, *Rapid Commun. Mass Spectrom.*, 2011, **25**, 140.
41 A. Vertes, *Springer Ser. Opt. Sci.*, 2007, **129**, 505.